Molecular Simulation of the Interaction of Diclofenac with Halogen (F, Cl, Br)-Encapsulated Ga$_{12}$As$_{12}$ Nanoclusters

Ikechukwu C. Nwobodo, Hitler Louis,* Tomsmith O. Unimuke,* Onyinye J. Ikenyirimba,
Anthony C. Iloanya, Gideon E. Mathias, Vincent N. Osabor, Eze F. Ahuekwe, and Adedapo S. Adeyinka

ACCESS | Metrics & More | Article Recommendations | Supporting Information

ABSTRACT: Diclofenac is one of the most frequently consumed over-the-counter anti-inflammatory agents globally, and several reports have confirmed its global ubiquity in several environmental compartments. Therefore, the need to develop more efficient monitoring/sensing devices with high detection limits is still needed. Herein, quantum mechanical simulations using density functional theory (DFT) computations have been utilized to evaluate the nanosensing efficacy and probe the applicability of Ga$_{12}$As$_{12}$ nanostructure and its engineered derivatives (halogen encapsulation F, Br, Cl) as efficient adsorbent/sensor materials for diclofenac. Based on the DFT computations, it was observed that diclofenac preferred to interact with the adsorbent material by assuming a flat orientation on the surface while interacting via its hydrogen atoms with the As atoms at the corner of the GaAs cage forming a polar covalent As−H bond. The adsorption energies were observed to be in the range of −17.26 to −24.79 kcal/mol and therefore suggested favorable adsorption with the surface. Nonetheless, considerable deformation was observed for the Br-encapsulated derivative, and therefore, its adsorption energy was observed to be positive. Additionally, encapsulation of the GaAs nanoclusters with halogens (F and Cl) enhanced the sensing attributes by causing a decrease in the energy gap of the nanocluster. And therefore, this suggests the feasibility of the studied materials as potentiometric sensor materials. These findings could offer some implications for the potential application of GaAs and their halogen-encapsulated derivatives for electronic technological applications.
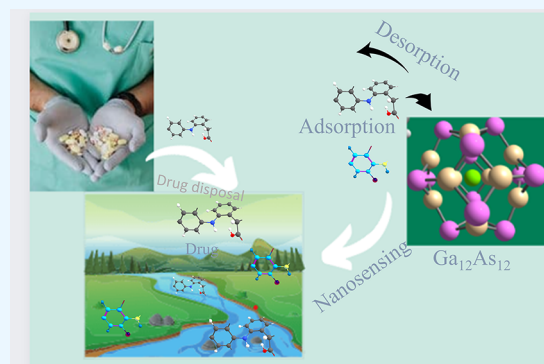
1. INTRODUCTION

Diclofenac (C$_{14}$H$_{11}$ClNO$_2$), a nonsteroidal benzene acetic acid derivative with potent anti-inflammatory activity, is mostly primed by acid-catalyzed cyclization of N-(2,6-dichlorophenyl)-α-(methyl sulfinyl) acetanilide. It was first synthesized by Alfred Sallman and Rudolf Fister in 1973[1] during a search for anti-inflammatory agents.[2] Diclofenac (DFN) is a constellate acid of diclofenac (-1).[3] As a result, diclofenac, a nonsteroidal anti-inflammatory medicine (NSAIM), binds and chelates with COX-1 and COX-2 variants, inhibiting arachidonic acid (AA); an essential fatty acid derived from omega-6, from being converted into proinflammatory prostaglandins (PG), physiologically vital eicosanoid. The DFN drug molecule and its active primary metabolite, 4′-hydroxydiclofenac (C$_{14}$H$_{11}$Cl$_2$NO$_3$), inhibit cyclooxygenase-1 and -2 enzymes, which are responsible for the production of prostaglandin (PG)-G$_2$, which is the precursor to other PGs. These molecules have a variety of active roles in pain and inflammation, and diclofenac's effects are all linked together by the reduction of their production. Although diclofenac is entirely absorbed from the gastrointestinal (GI) tract, only 60% of the medication reaches the blood vessels unaltered,

suggesting that there is likely significant initial metabolism.[4] DFN is predominantly lost by metabolism, as 60−70% of it is excreted in the urine and 30% is eliminated in feces. It undergoes oxidative metabolism to hydroxyl metabolites as well as complexation to glucuronic acid, sulfate, and glutamate. Thus, PGE$_2$ activation causes the hypothalamus's thermoregulatory neurons, which serve as excitatory receptors, to create more heat and less heat loss, which results in fever. As such, DFN as an NSAID prevents the generation of PGE$_2$ through the activity of these neurons. In July 1988, the Food and Drug Administration (FDA) of the United States conferred its initial approval for use under the brand name Voltaren to treat pain and inflammation from a variety of causes, including nociceptive ailments like rheumatoid arthritis and osteoarthritis as well as injury-related inflammations brought on

by surgery and physical trauma, etc.[5] Though it is sufficient to maintain various inflammation and limit the production of prostaglandin at the site of injury by reducing inflammation, it has some adverse effects on the human body as it can increase the risk of developing gastrointestinal ulcers by inhibiting the production of protective mucus in the stomach. As membrane lipoproteins are broken down by phospholipase A2 to eicosanoids, the substrate for the COX enzymes, the side effect of the DFN medication is compared to this process. While COX-2 is significantly upregulated during times of inflammation, it causes vasodilation and inflammation through the migration of macrophages, fibroblasts, and macrophages. COX-1 is constitutively expressed in the stomach, kidneys, and intestinal endothelium, where it causes vasoconstriction and platelet aggregation. As a result, the equilibrium between the specific enzymes is ultimately altered when NSAIDs are taken. Diverse studies have revealed that DFN is the most common NSAID drug responsible for vascular and coronary risk. In a study involving ibuprofen, naproxen, coxib, and diclofenac, it was reported that major adverse cardiovascular events (MACEs) were increased by about a third by DFN, majorly because of an increase in major coronary events.[6] Additionally, although they only sometimes are presented with symptoms, mental health side effects have been documented and are therefore considered to be potential adverse effects of DFN.[7] In tandem, its ecological effect is not also in any way left behind; as studies have also revealed that the use of DFN for animals is highly controversial due to its toxicity when eaten by scavenging arboreal and aquatic organisms,[8] as the medication has been priorly banned for veterinary use in several countries, as it has adversely led to a sharp decline in the population of aquatic and arboreal habitat organisms, majorly in the Indian subcontinent.[9] Thus, as a large observational study, although it has certain adverse effects, this medication is required to treat pain, inflammatory illnesses, and dysmenorrhea spurred by a variety of different causes.[10] As a result, the detection of the DFN drug is crucial and will confront severe requirements to eliminate these side effects.

It is critical to understand that nanostructured materials are substances with nanoscale dimensions that can be one, two, three, or zero (often between 1 and 100 nm). Examples of these structures include nanoclusters, nanosheets, nanotubes, and nanocages.[11] A remarkable appeal to nanostructured materials by the scientific research community after the sensitization of two-dimensional graphene structure was given by Novoselov et al.[11] Given their biocompatibility, low toxicity, reduced cost, and titillating mechanical and electrical features, nanoclusters as nanostructured materials are heavily investigated for nanoscale drug sensing and drug delivery vehicles.[12−14] As recorded in the past few years, it has been revealed via experimental and theoretical studies that pure semiconductor-based nanostructures can be used as sensors for various lethal drugs and hazardous gases.[15] For instance, Li et al. studied the Ga surface as a reliable glucose detector using a broad experimental and theoretical approach.[16] They developed a gallium-based biosensing platform that was supported by enzymes/proteins on the gallium surface. To date, numerous researchers from various research groups have conducted several experimental studies to detect drugs, such as doxorubicin, allopurinol, metronidazole, ibuprofen, etc., using a nanostructured gallium encapsulated-graphite carbon nitride (g-C_3N_4). They have produced promising results that will be used in clinical settings.[17] Accordingly, Tonel et al. carried out

a theoretical study in which they intriguingly discovered physisorption interaction between a nano-based pristine graphene nanosheet and the anticancer drug doxorubicin with the binding energy of 0.49 eV, and they consequently demonstrated a decrease in the interaction with increasing temperature using DFT theory in a SIESTA code with a GGA-PBE functional.[17] More so, a gallium-doped fullerene (C_{24}) nanocage has been proposed as a potent sensing nanostructure for Melphalan anticancer drug by carrying out DFT at the B3LYP/6-31G(d) level of theory by Mirkamali et al.[18] Finally, Veeralingam et al. experimentally projected and showed a two-dimensional metallic $NiSe_2$ nanocluster-based low-cost amperometric material as a sensor for detecting neurological drug carbamazepine in human sweat.[19] Thus, with numerous advances in nanoscience, researchers have set themselves to discover the unique properties of semiconductor nanostructures, in which GaAs is one used for the purpose of applying them in diverse fields. Semiconductor nanostructures have distinctly emerged as potential candidates in the field of sensing and transporting drugs in target sites for their worthwhile properties, including chemical and thermal stability and wide-ranging band gap compared to their other non-semiconductor-based counterparts. Yen's team developed a hybrid GaAs-based device successfully for sensing hemoglobin (Hb) in biological solutions. As such, the GaAs nanosensor could detect Hb in swine intestinal fluids (SWIFs) with greater sensitivity.[20,21]

Hitherto, a comparative analysis has been carried out by performing quantum mechanical calculations on the premise of density functional theory to develop an effective, affordable, and environmentally friendly nanosensor to detect DFN drugs. The prolific factors for the adsorption of DFN drug on halide (Cl, F, Br)-encapsulated GaAs nanoclusters were investigated. To the optimum best of our knowledge, there has been no theoretical study on the interaction of DFN drugs with the encapsulated nanoclusters. DFN is a commonly consumed anti-inflammatory agent; thus, the possibility of exhibiting adverse effects, when disposed to aquatic and nonaquatic environments, is considerably high based on demographic surveys. Hence, our pivotal aim is to identify an auspicious DFN drug sensor by studying its geometric structures; electronic, topological, and adsorption characteristics; and sensing mechanism.

2. COMPUTATIONAL DETAILS

All computations performed in this study were based on density functional theory (DFT). The optimum model employed for computations including geometry optimization was the ωB97XD functional with the def2-SVP basis set. The essence of choosing this functional and basis set is due to its ability to identify both long-range and short-range interactions; however, the inclusion of D2 dispersion correction enhances the accuracy of computations considerably by considering all forms of interactions. Also, this combined level of theory can model the molecular orbitals of carbon, Ga, As, nitrogen, and oxygen atoms with much accuracy. Moreover, the data obtained from several benchmark studies are good evidence of this reality.[22,23] The D2 empirical dispersion from Chai and Martin[23] is very successful in describing intermolecular forces. The computational code deployed for all computations was the Gaussian 16 code.[24] Substantial accuracy has been ensured during the optimization process such that the mesh has been selected for very intensive integration to increase the accuracy
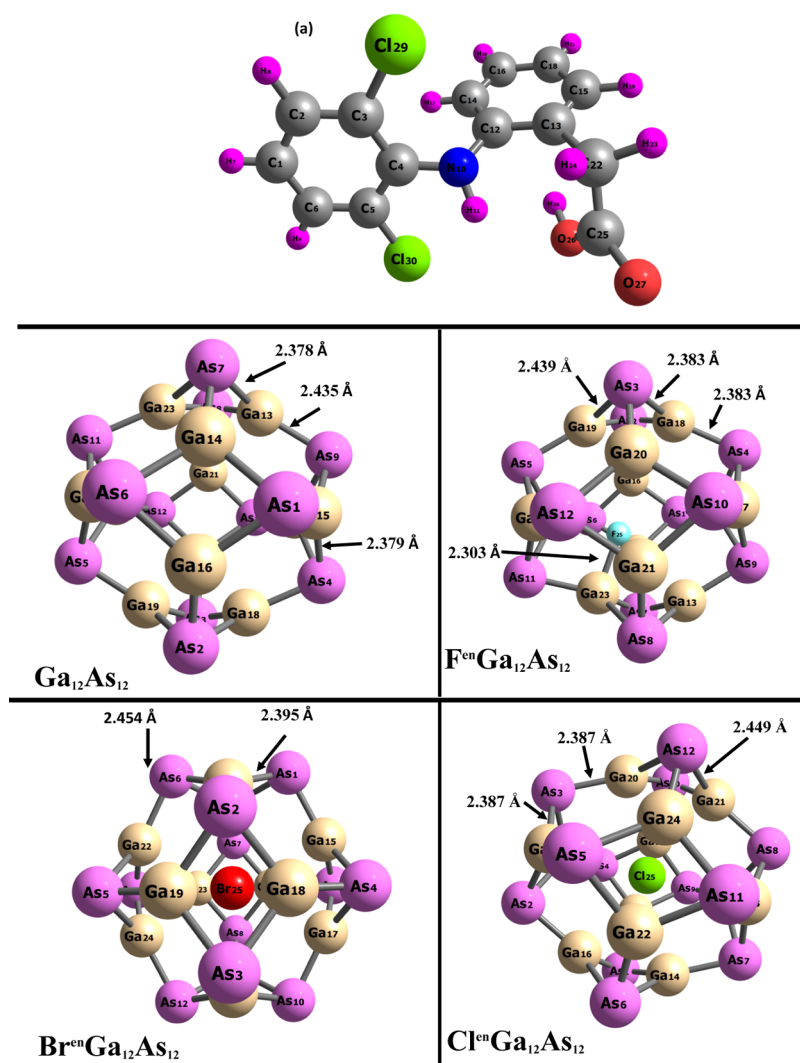
Figure 1. Relaxed geometry of the studied adsorbate (a) and nanocages. Geometry relaxed at the DFT/ωB97XD/def2-SVP level.

of the computations. Also, to ascertain that the final optimized geometry corresponds to a minimum, the necessary measures with regard to frequency computations were adhered and computed as appropriate. The absence of imaginary frequencies as obtained is an affirmation of the true correlation of the optimized structures to their corresponding local minimum on the potential energy surface. Also, the stability of the wave function simulated separately further affirms the accuracy of the computations and results reported herein. The NBO software version 3.1,[25] Multiwfn_dev_7.1,[26] Gauss-Sum,[27] and Visual molecular dynamics[28] packages were utilized for wave function analyses and diagrammatic illustrations. For accurate computations of adsorption energies, basis set superposition error (BSSE) was calculated separately by running single-point energy calculations on the optimized complexes with the inclusion of counterpoise correction.[29−33] The formula for computation of adsorption energy is given as thus

$$E_{ad} = E_{complex} - E_{adsorbate} - E_{adsorbent} + E_{(BSSE)} \qquad (1)$$

where $E_{complex}, E_{adsorbate}$, and $E_{adsorbent}$ are the total energies of the adsorbed complex, diclofenac, and GaAs nanoclusters, respectively. The BSSE energies and complexation energies are reported in the Supporting Information.

3. RESULTS AND DISCUSSION

**3.1. Geometry Optimization and Attainment of Stability.** The geometries of the studied nanostructured materials were optimized at the ωb97XD/def2-SVP level of computations. However, to first ascertain the best adsorption configuration, different adsorption modes were tested. This is because multiple adsorption sites are available on the surface of the nanostructured materials, and hence, adsorption of adsorbate molecules must not occur at random sites but at specific sites with the highest affinity and propensity to ensure the overall stability of the surface and the adsorbate after adsorption. Therefore, it is pertinent to search for these sites that ensure maximum stability of both adsorbate and adsorbent prior to adsorption. To effectively ensure these, the adsorbing molecule (diclofenac) was separately optimized at the chosen level of computations and then placed at a suitable orientation with the Ga$_{12}$As$_{12}$ nanosurface and its encapsulated derivatives for maximum interactions. However, for the sake of accuracy and ease, the Molclus software program was invoked to do the search for stable adsorption configuration. This program utilizes artificial intelligence to scout for favorable adsorption conformations while ranking the best conformation based on the obtained energy of interaction. Figure 1 depicts the optimized geometry of diclofenac and the nanostructured
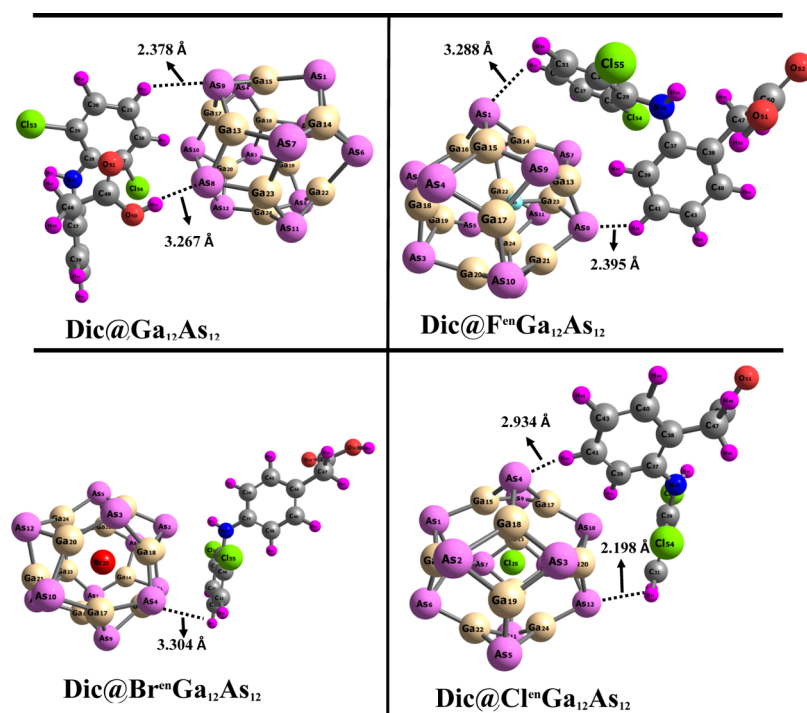
Figure 2. Relaxed geometry of the stable adsorption configurations of Dic on the respective nanoclusters. Geometry relaxed at the DFT/ωB97XD/def2-SVP level.

materials, while Figure 2 discloses the best adsorption configuration of diclofenac with the nanosurfaces under consideration as predicted by Molclus software after proper geometry optimization. The studied $Ga_{12}As_{12}$ nanosurface is mainly enclosed by eight hexagonal rings and six tetragonal facets, which modulates into a nonperiodic cage-like material as depicted in Figure 3. The geometric parameters are outlined
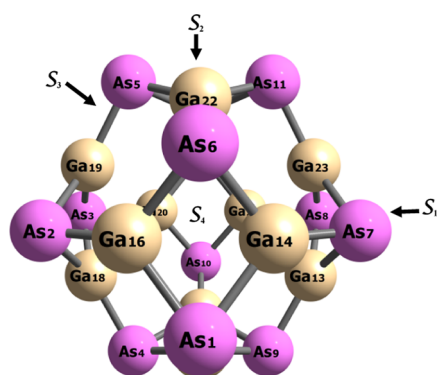
Figure 3. Four feasible adsorption sites of the nanocluster. The adsorbent is placed on top of the As atom (S_1), on top of the Ga atom (S_2), on top of the bond r^{66} in-between Ga and As (S_3), and on top of the tetragonal ring r^{64} (S_4).

in Table 1. Similarly, the Ga−As bond is composed of two bond types: the Ga−As bonds of the hexagonal facet linking the tetragonal and the Ga−As bond connecting two tetragonal ring facets. These are designated as r^{66} and r^{64}, respectively, for hexagonal and tetragonal rings. Therefore, the bond connecting two tetragonal rings r^{64} (As_1-Ga_{15}) was observed to possess a bond length of 2.379 Å, the bond in-between two tetragonal facets (As_7-Ga_{14}) is calculated to be 2.435 Å, and the bond between two hexagonal facets ($Ga_{14}-As_7$) exhibited a

bond length of 2.378 Å. It has been established that varying adsorption configurations were considered during the adsorption process; these sites were on the r^{64} bonds, r^{66} bonds, on the center of the tetragon, on the center of the hexagonal, in close proximity with Ga as well as As atoms. Nonetheless, at the end of the optimization and search for stable geometry, it was observed that the adsorbate (Dic) preferred to be adsorbed at the As active sites by forming weak physisorption bonds via the hydrogen atoms of the aromatic ring (mostly H_{34}) and As_4 and As_9 atoms, respectively, as projected in Table 1. Of course, this observation is prompted by the electropositive nature of the hydrogen atoms due to the electron density difference between the aromatic circle and the proton, therefore making them more sensitive to the highly electronegative As atoms of the nanoclusters. However, slight changes in bond geometry were observed after adsorption on specific sites. Both r^{64} and r^{66} bonds in Dic@$F^{en}Ga_{12}As_{12}$ are observed to slightly increase in bond length by 0.016 and 0.062%, respectively. This elongation in bond geometry is obviously the result of substantial charge transport between the adsorbate and adsorbent surface. This is affirmed by the negative charges assumed by the nanoclusters, as reported in Table 2, except for the non-encapsulated $Ga_{12}As_{12}$ nanocluster, which maintains a positive charge. The positive nature of the charge assumed by this nanocluster further accounts for the resistance to changes in bond geometry as observed. Nonetheless, the nanoclusters resisted deformations by bond breaking or dramatic changes in both the tetragonal and hexagonal facets, which forms the entire nanocage. Moreover, the charge and multiplicity of the nanoclusters were maintained at -1e and singlet, respectively, thus, stabilizing the nanoclusters considerably.

3.2. Electronic Properties. Electronic properties, such as electron affinity (EA), energy gap (E_g), electronegativity (χ), ionization potential (IP), etc., as evaluated by Koopmans

Table 1. Geometric Parameters of the Complexes: Adsorption Bond Length (d_{ads}), Bond Length between Two Tetragonal Facets (r^{64}), and Bond Length between a Tetragonal and Hexagonal Facet (r^{66})[a]

structure	d_{ads}	Å	r^{64}	Å	r^{66}	Å
$Ga_{12}As_{12}$			$Ga_{15}-As_1$	2.379	$Ga_{14}-As_7$	2.435
$F^{en}Ga_{12}As_{12}$			$Ga_{16}-As_2$	2.383	$Ga_{19}-As_5$	2.360
$Cl^{en}Ga_{12}As_{12}$			$Ga_{15}-As_1$	2.387	$Ga_{16}-As_2$	2.388
$Br^{en}Ga_{12}As_{12}$			$Ga_{20}-As_3$	2.394	$Ga_{19}-As_5$	2.395
$Dic@Ga_{12}As_{12}$	As_9-H_{31}	2.378	As_1-Ga_{15}	2.379	As_1-Ga_{14}	2.433
	As_9-H_{31}	3.267				
$Dic@F^{en}Ga_{12}As_{12}$	As_1-H_{32}	3.288	$Ga_{15}-As_9$	2.399	As_9-Ga_{13}	2.422
$Dic@Cl^{en}Ga_{12}As_{12}$	As_4-H_{45}	2.934	$Ga_{12}-As_{21}$	2.447	$Ga_{18}-As_4$	2.389
	$As_{12}-H_{32}$	3.198				
$Dic@Br^{en}Ga_{12}As_{12}$	As_4-H_{34}	3.304	As_2-Ga_{18}	2.451	As_2-Ga_{16}	2.394

[a]Computed at the ωB97XD/def2-SVP level.

**Table 2. Electronic Properties of the Modeled Systems[a]**

structures	HOMO(eV)	LUMO (eV)	E_g (eV)	IP (eV)	EA (eV)	E_{FL} (eV)	η (eV)	σ (eV)	ω (eV)	χ (eV)
$Ga_{12}As_{12}$	−7.899	−2.379	5.519	−7.899	−2.379	−5.139	−2.759	−0.362	−36.448	5.139
$F^{en}Ga_{12}As_{12}$	−4.865	−0.817	5.682	−4.865	0.817	−2.024	−2.841	−0.352	−5.822	2.024
$Cl^{en}Ga_{12}As_{12}$	−4.976	−0.882	5.858	−4.976	0.882	−2.048	−2.929	−0.341	−6.135	2.047
$Br^{en}Ga_{12}As_{12}$	−4.9963	−0.8395	5.836	−4.996	0.839	−2.078	−2.918	−0.342	−6.302	2.078
$Dic@Ga_{12}As_{12}$	−7.902	−2.368	5.534	−7.902	−2.368	−5.135	−2.767	−0.361	−36.479	5.135
$Dic@F^{en}Ga_{12}As_{12}$	−5.034	−0.653	5.686	−5.034	0.653	−2.190	−2.843	−0.352	−6.821	2.190
$Dic@Cl^{en}Ga_{12}As_{12}$	−4.618	−0.130	4.488	−4.618	−0.130	−2.374	−2.244	−0.446	−6.325	2.374
$Dic@Br^{en}Ga_{12}As_{12}$	−4.444	−0.067	4.376	−4.444	−0.067	−2.255	−2.188	−0.457	−5.566	2.255

[a]Energy gap (ΔE, [eV]), ionization potential (IP, [eV]), electron affinity (EA, [eV]), chemical hardness (η, [eV]), chemical softness (μ, [eV]) chemical potential (μ, [eV]), electrophilicity (ω, [eV]), and electronegativity (χ, [eV]).

approximation, are carefully computed in Table 2. These parameters provide detailed insight into the conductivity and stability of the nanomaterials and aid in the comprehension of the diverse mechanism of adsorption as well as changes in structural rearrangement due to adsorption. It can be deduced from Table 2 that the energy gap of the clean surface $Ga_{12}As_{12}$ was observed to be 5.5196 eV. However, upon encapsulation with selected halogens, the energy gap of the complexes slightly increases to 5.8575, 5.835, and 5.6820 eV, respectively, for $Cl^{en}Ga_{12}As_{12}$, $Br^{en}Ga_{12}As_{12}$, and $F^{en}Ga_{12}As_{12}$. Interestingly, it was further observed that upon adsorption with diclofenac (dic), a slight increase of 0.014 eV was observed. In contrast, adsorption of diclofenac on the encapsulated structures causes a corresponding decrease in energy gap. The energy gaps of chlorine- and bromine-encapsulated surfaces (Dic@$Cl^{en}Ga_{12}As_{12}$ and Dic@$Br^{en}Ga_{12}As_{12}$) were calculated to be 1.369 and 1.4594 eV, respectively. The adsorption of diclofenac on the $F^{en}Ga_{12}As_{12}$ (Dic@ $F^{en}Ga_{12}As_{12}$) surface obstructed the usual trend, as a slight increase in energy gap of about 0.0044 eV was observed. This trend suggests that encapsulation of the proposed nanosensor surface led to a greater stability with less conductivity as explicated by the sudden increase in energy gap. Also, the Fermi level (E_{FL}) of the clean surface $Ga_{12}As_{12}$ was observed to be −5.139 eV upon encapsulation with selected halogens. A dramatic decrease in the Fermi level energy of about −3.061 to −3.115 eV was observed because of encapsulation. Nevertheless, adsorption of diclofenac on the sensor surface slightly elevated the Fermi energy level of the halogenated system as the Dic@ $Cl^{en}Ga_{12}As_{12}$ complex appears to possess the highest Fermi energy level of −2.3742 eV, as reported in Table 2 which correlate with the chemical hardness (η) of 2.244 eV and chemical softness (S) of −0.4456 eV, respectively. From Table

1 the adsorption distance also reveals that Dic@$Cl^{en}Ga_{12}As_{12}$ and Dic@$Ga_{12}As_{12}$ nanosensor surfaces had the shortest distance of 2.934 and 2.378 Å between As_4-H_{45} and As_9-H_{31} adsorption sites compared to other systems. Thus, there is a comparably stronger interaction between the encapsulated chlorine atom and the adsorbate (Dic@$Ga_{12}As_{12}$) nanostructure, with high stability and less conductivity, which would thus enhance the sensing property of this engineered nanosensor surface (Dic@$Cl^{en}Ga_{12}As_{12}$) in detecting diclofenac (see Figure 4).

3.3. Natural Bond Orbital (NBO) Analysis. To properly validate and quantify the exact strength of interaction as well as amount of charge being transferred from the nanosurfaces to the adsorbate and vice versa, as well as comprehend all electronic rearrangement and stabilizations, the natural bond orbital investigation is deployed to this effect. NBO effectively quantifies the exact amount of charge transfer between the respective donor and acceptor orbitals in the form of Lewis and non-Lewis delocalization,[34] thereby enabling the mechanism of molecular reorganizations because of adsorption to be visualized. Based on this premise, the stabilization and intermolecular reorganization as a result of Dic adsorption on the surfaces of the engineered nanostructured materials are investigated by wholistically observing the second-order stabilization energy (E^2) orchestrated by various donor–acceptor molecular interactions. This energy serves as a measure of interaction strengths and serves as an index of stability upon adsorption. The NBO analysis is calculated at the DFT/ωB97XD/def2-SVP level. The obtained results are reported in Table 3. The stabilization energy of the clean surface Dic@$Ga_{12}As_{12}$ resulted from the interaction between LP(1)$As_9 \rightarrow \sigma^*C_{25}-H_{31}$. The E^2 amounted to 72.44 kcal/mol for this interaction, whereas a total of 180.10 kcal/mol was
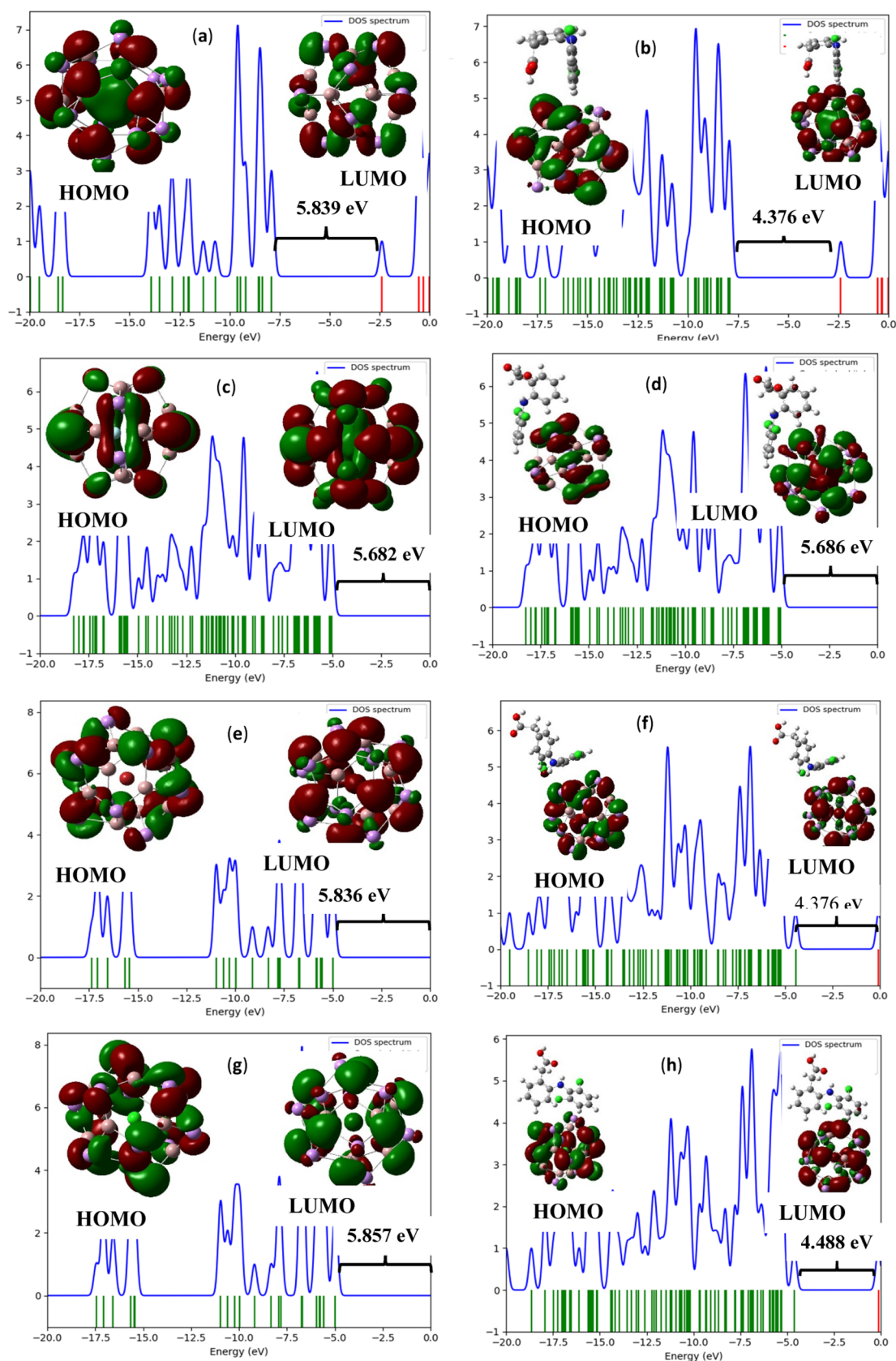
Figure 4. Density of state map showing energy gap as well as molecular orbital isosurface maps for the studied systems, respectively. (a−h) $Ga_{12}As_{12}$, $Dic@Ga_{12}As_{12}$, $F^{en}Ga_{12}As_{12}$, $Dic@F^{en}Ga_{12}As_{12}$, $Cl^{en}Ga_{12}As_{12}$, $Dic@Cl^{en}Ga_{12}As_{12}$, $Br^{en}Ga_{12}As_{12}$, and $Dic@Br^{en}Ga_{12}As_{12}$.

observed as total stabilization energy among the selected stabilization interactions within this complex. However, the

stabilization interactions within the encapsulated complexes $Dic@F^{en}Ga_{12}As_{12}$, $Dic@Br^{en}Ga_{12}As_{12}$, and $Dic@Cl^{en}Ga_{12}As_{12}$

Table 3. Intramolecular Donor–Acceptor Interactions and Second-Order Stabilization Energies of the Most Interacting NBOs of the Complexes Obtained at the DFT/ωB97XD/def2-SVP Level

donor NBO (i)	acceptor NBO (j)	E^2, kcal/mol	$E(j) - E(i)$, au	$F(i,j)$, au
	Dic@Ga$_{12}$As$_{12}$			
LP(1)As$_9$	σ^*C$_{25}$–H$_{31}$	72.44	1.23	0.277
ΠC$_{25}$–C$_{30}$	Π^*C$_{26}$–C$_{27}$	40.98	0.37	0.111
LP(1)N$_{34}$	Π^*C$_{28}$–C$_{29}$	24.98	0.43	0.100
LP(2)O$_{51}$	σ^*C$_{49}$–O$_{50}$	41.70	0.66	0.150
	Dic@Br^{en}Ga$_{12}$As$_{12}$			
LP(1)As$_1$	σ^*C$_{27}$–H$_{33}$	143.56	1.14	0.373
LP(4)Br$_{25}$	LP*(1)Ga$_{16}$	22.50	0.41	0.088
ΠC$_{26}$–C$_{31}$	Π^*C$_{27}$–C$_{28}$	40.20	0.38	0.112
ΠC$_{27}$–C$_{28}$	Π^*C$_{29}$–C$_{30}$	42.82	0.37	0.116
	Dic@Cl^{en}Ga$_{12}$As$_{12}$			
LP(1)As$_{12}$	σ^*C$_{26}$–H$_{32}$	130.61	1.13	0.354
ΠC$_{26}$–C$_{31}$	Π^*C$_{27}$–C$_{28}$	39.21	0.36	0.108
LP(2)O$_{51}$	Π^*C$_{50}$–O$_{52}$	41.72	0.48	0.128
LP(3)Cl$_{54}$	σ^*C$_{47}$–H$_{48}$	17.10	0.99	0.119
	Dic@F^{en}Ga$_{12}$As$_{12}$			
LP(1)As$_1$	σ^*C$_{26}$–H$_{32}$	96.60	1.18	0.313
LP(3)Cl$_{54}$	Π^*C$_{38}$–C$_{40}$	59.51	0.55	0.172
ΠC$_{26}$–C$_{31}$	Π^*C$_{27}$–C$_{28}$	42.63	0.36	0.112
LP(2)O$_{52}$	σ^*C$_{50}$–O$_{51}$	40.41	0.67	0.148

were observed to be 96.60, 143.56, and 130.61 kcal/mol, respectively, resulting from the delocalization of LP(1)As$_1$ → σ^*C$_{26}$–H$_{32}$, LP(1)As$_1$ → σ^*C$_{27}$–H$_{33}$ and LP(1)As$_1$ → σ^*C$_{26}$–σ^*C$_{26}$–H$_{32}$. Notably, the interactions between the lone pair donor orbitals and σ antibonding acceptor orbitals are the dominant stabilization interactions with comparably higher stabilization energy. These interactions are also evidence of the charge transfer occurring between the adsorbate and the nanocluster. These interactions occur at the catalytic site of interaction and therefore affirm the sensitivity of the nanocluster toward the studied adsorbate and portray the exact amount of charge being transferred as a result of adsorption. The reported values show that encapsulation with halogens elevated the stabilization energy, i.e., encapsu-

lation enhances the sensitivity of the nanocluster considerably. A closer inspection of the stabilization interactions shows that Dic@Br^{en}Ga$_{12}$As$_{12}$ and Dic@Cl^{en}Ga$_{12}$As$_{12}$ exhibited the highest E^2 energies, which might result from a better orbital overlap between the adsorbed molecule and the surface, which is in line with previous reports. Also, the results divulged that the Br- and Cl-encapsulated surfaces are more sensitive toward the Dic molecule, and the interaction exhibited are considerably stronger than the F-encapsulated derivatives. A further evaluation of the strength of interaction would be explained by the quantum theory of atoms in molecules.

3.4. Projected Densities of State. The densities of states of systems are quite vast in explicating interesting electronic structure properties of materials. It is perhaps the most essential concept that provides a simplified approach to effectively comprehend complex physical and electronic properties.[34,35] Electronic properties ranging from optical, electrical, and band structures are visually apparent from projected densities of state (PDOS). Thus, the notion of DOS becomes very essential to gain substantial insights into electronic structure and reorganization of electronic bands and energies as a result of adsorption or encapsulation. The effect of halogen encapsulation on the electrical and band energies of the studied nanoclusters can as well be better explained by DOS maps. The projected density of state maps for the interaction of Dic with the respective nanoclusters is depicted in Figure 5. The remarkable features of the electronic structure that are perceptible from the DOS maps are revealed via band shapes; a closer inspection of the DOS maps shows two distinct peaks: a sharp band and several parabolic bands. The parabolic bands clearly show the energy dependence of DOS and clearly show that the conduction quantum states are dominated by contributions from the electrons of the nanosurface (Ga$_{12}$As$_{12}$) and these contribute a greater percent to the TDOS. These bands are also significantly enhanced by halogen encapsulation. The sharp cylindrical band at −0.7 au is a characteristic of a 2D electronic structure and depicts Van Hove singularities, which are responsible for the optical alertness of materials. The DOS spectrum also affirms the presence of charge transfer from the conduction band of the nanocluster to the valence bands of the adsorbate molecule. To
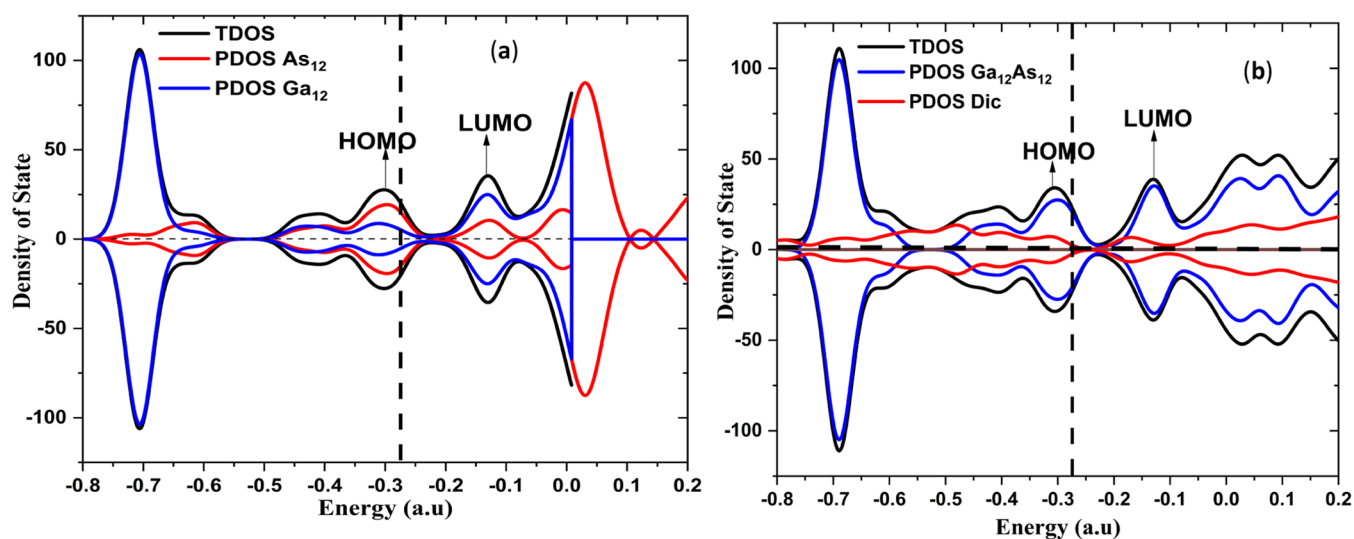
Figure 5. Projected density of states for the interacted nanoclusters: (a) Ga$_{12}$As$_{12}$ and (b) Dic@Ga$_{12}$As$_{12}$.

Table 4. E_{ad} (Adsorption Energy in kcal/mol), ΔH (Enthalpy in kcal/mol), ΔG (Gibb's Free Energy in kcal/mol), ΔS (Entropy in cal mol^{-1} K^{-1}), E_{def} (Deformation Energy kcal/mol), and $Q(\acute{e})$ Amount of Charge Transferred during Adsorption

modeled systems	E_{ad}(kcal/mol)	ΔH	ΔG	ΔS	$E_{def.}$	$Q(\acute{e})$
Dic@Ga$_{12}$As$_{12}$	−17.26	197.98	92.02	355.39	51.16	0.6955
Dic@F^{en}Ga$_{12}$As$_{12}$	−18.66	−46.44	−34.05	269.99	61.18	−0.97147
Dic@Br^{en}Ga$_{12}$As$_{12}$	89.72	44.05	34.63	321.23	61.20	−0.86402
Dic@Cl^{en}Ga$_{12}$As$_{12}$	−24.79	−55.18	−41.09	299.01	1.86	−0.99189

this end, the PDOS of the nanocluster has been separately visualized to understand and visualize the exact origin of the charge being transferred and affirm the catalytic sites of adsorption. As revealed in Figure 5, the PDOS for the GaAs nanocluster is characterized by a dominance of electronic densities from the Ga atoms at the occupied states, while As atoms contribute a greater percentage at the virtual state. This is visible by the sharp band beyond the nonzero energy level of the DOS map. However, the HOMO density is dominated by the As electronic state, while the LUMO is dominated by major contributions from the Ga atoms. This affirms why the adsorbate prefers to interact via flat orientation with the nanosurface.

3.5. Adsorption Studies. To further affirm the feasibility and suitable adsorption conformation of the interaction between Dic and the nanosurfaces, adsorption energy and thermodynamics of adsorption are undertaken to this end. The energies have been computed at the same level of theory as the optimization model considering basis set superposition error by counterpoise corrections. Adsorption enthalpies could also pivot the strength as well as energetics of the sensitivity of the surfaces toward the considered adsorbate molecule. The computed adsorption enthalpies and thermodynamics of adsorption are depicted in Table 4, and the adsorption energies (E_{ads}) were computed using eq 1. It is ostensible from the computed results in the table that all adsorption enthalpies are negative, thus suggesting the stable adsorption process. Moreover, the thermodynamics of adsorption, such as enthalpy of adsorption (ΔH), Gibb's free energy of adsorption (ΔG), and entropy of adsorption (ΔS), also present negative enthalpies and free energies of adsorption while all energetics from entropic considerations are positive. These negative energies demonstrate the spontaneous nature of the adsorption process. The adsorption energies were all observed in the range of −0.16 to −0.36 eV, which were all in the physisorption range. Nonetheless, encapsulation of the nanocluster with halogens causes substantial disruption in the regular symmetry of the nanocluster. This is evident in the slight increase in adsorption energy of the encapsulated nanoclusters. The computed adsorption energy of F- and Cl-encapsulated surfaces exhibited negative adsorption energies, whereas the Br-encapsulated surface disclosed positive adsorption energy due to considerable deformation in structure because of the strong interaction of the adsorbate molecule with this nanosurface. Moreover, the least electronegativity of the Br atom could also be the direct consequence of the less affinity of the surface toward the adsorbate and hence the drastic change in adsorption energy. To further affirm this reality, the deformation energies of the nanoclusters have been computed as reported in Table 4. In all cases, the Cl-encapsulated nanosurface exhibited the lowest deformation, whereas the Br- and F-encapsulated nanosurfaces expressed the highest deformation energy due to stronger interactions with the surface. However, the negative enthalpy of adsorption of the F-

encapsulated nanosurface shows that the adsorption is stable and favorable, and also the thermodynamic considerations further affirm the exothermic nature of the adsorption process in F- and Cl-encapsulated surfaces. During the adsorption process, substantial charge was transferred from the nanocluster (Ga$_{12}$As$_{12}$) to the adsorbate molecule (Dic). This is expressed by NBO charge; the charge transfer could arise because of the electronegative atoms present in the adsorbate molecule, which pushes the electron density toward the adsorbate molecule. This is in tandem and consistent with other electronic properties as previously explained. Hence, the most stable geometrical configuration (Dic@Cl^{en}Ga$_{12}$As$_{12}$), as exhibited in Table 4 is such oriented such that the adsorbate atoms are flat on the nanosuface, and the adsorption distance is approximately between 2.934 and 3.198 Å compared to other configurations. Based on this premise, it could be deduced that the most favorable configuration of the Dic molecule on the nanosurfaces is in the order Dic@Cl^{en}Ga$_{12}$As$_{12}$ > Dic@F^{en}Ga$_{12}$As$_{12}$ > Dic@Br^{en}Ga$_{12}$As$_{12}$, prompting that encapsulation significantly enhances the sensitivity of the surface toward the adsorbed molecule. To confirm the environmental effects of the studied nanoclusters on aquatic and arboreal habitat and their organisms, a concrete literature survey is undertaken to this end. According to the report by Nguyen et al.,[36] on ecotoxicity of GaAs, InAs, Ga$_2$O$_3$, and In$_2$O$_3$ nanoparticles, the toxicity induced by arsenide under environmental conditions will vary depending on intrinsic properties of the material, such as particle size, as well as on the dissolution time and aqueous chemistry. According to another report by Zeng et al.,[37] on the ecotoxicity of As(III), As(V), In(III), and Ga(III) species and on marine bacterium *Aliivibrio fisheri* and *Daphnia magna* species, the toxicity of these species depended on the sensitivity of the organisms toward the studied metals, Ga and In particularly were mildly toxic during the experiments, and *D. magna* was the most sensitive organism for In and Ga with 50% lethal concentrations of 0.5 and 3.4 mM, respectively. More so, the 50% inhibitory concentrations of both arsenic species toward methanogens were about 0.02 mM, which is lower than the regulated maximum allowable daily effluent discharge concentration (2.09 mg/L or 0.03 mM) for facilities manufacturing electronic components in the US. Nevertheless, due to the intended use of the studied materials as potentiometric sensors and not voltammetric sensors, the probability of these impending environmental concerns is limited.

3.6. Quantum Theory of Atoms in Molecules (QTAIM). QTAIM is a topology analysis proposed by Bader for the investigation of intramolecular interactions and intermolecular interactions.[38] A critical point offers insight into the features of the interactions using the topological parameters. In topological analysis, covalent, noncovalent, and partially covalent interactions are the only interactions of concern. However, noncovalent nature of interaction consists of electrostatic, hydrogen bonding, and van der Waal's

Table 5. QTAIM Parameters for the Modeled Surfaces under Investigation Providing Insights into the Bond Critical Points of the Complexes[a]

bond	BCP	$\rho(r)$	$V^2\rho(r)$	$V(r)$	$K(r)$	$G(r)$	ε	ELF	$H(r)$
				Dic@Ga$_{12}$As$_{12}$					
Ga$_{21}$−Cl$_{54}$	128	0.0089	0.0172	−0.0040	0.0001	0.0038	1.1323	0.0709	−0.0001
As$_9$−H$_{31}$	58	0.0045	0.0129	−0.0014	−0.0008	0.0024	0.0600	0.0218	0.0008
As$_{10}$−H$_{32}$	100	0.0078	0.0216	−0.0032	−0.0011	0.0043	1.1352	0.0397	0.0011
As$_8$−H$_{52}$	115	0.0151	0.0312	−0.0080	0.0001	0.0079	0.0248	0.1012	−0.0001
				Dic@Br^{en}Ga$_{12}$As$_{12}$					
As$_2$−Cl$_{54}$	89	0.0049	0.0108	−0.0020	−0.0003	0.0024	2.4260	0.0274	0.0003
As$_4$−Cl$_{55}$	105	0.0040	0.0091	−0.0016	−0.0003	0.0019	1.1230	0.2084	0.0003
As$_2$−H$_{36}$	122	0.0125	0.0343	−0.0066	−0.0010	0.0076	0.1928	0.0611	0.0010
As$_4$−C$_1$	71	0.0070	0.0180	−0.0030	−0.0008	0.0037	0.0737	0.0375	0.0008
Br$_{25}$−Ga$_{15}$	91	0.0146	0.0274	−0.0072	0.0009	0.0063	0.2460	0.1219	−0.0009
				Dic@Cl^{en}Ga$_{12}$As$_{12}$					
As$_3$−Cl$_{54}$	134	0.0060	0.0127	−0.0026	−0.0003	0.0029	0.0266	0.0380	0.0003
As$_{10}$−H$_{42}$	104	0.0057	0.0153	−0.0020	−0.0009	0.0029	0.2231	0.0310	0.0009
Ga$_{20}$−C$_{32}$	78	0.0071	0.0172	−0.0029	−0.0005	0.0034	0.3629	0.0429	0.0005
Ga$_{17}$−H$_{45}$	172	0.0082	0.0217	−0.0034	−0.0010	0.0044	0.1410	0.0453	0.0010
Ga$_{23}$−Cl$_{25}$	95	0.0122	0.0245	−0.0062	0.0006	0.0056	0.3184	0.0872	−0.0006
				Dic@F^{en}Ga$_{12}$As$_{12}$					
As$_7$−Cl$_{54}$	121	0.0059	0.0128	−0.0026	−0.0003	0.0029	0.2467	0.0351	0.0311
As$_9$−C$_{29}$	127	0.0039	0.0104	−0.0013	−0.0006	0.0020	2.8631	0.0189	0.0006
As$_7$−H$_{33}$	141	0.0062	0.0186	−0.0024	−0.0011	0.0035	0.5082	0.0284	0.0011
As$_8$−H$_{45}$	68	0.0040	0.0114	−0.0013	−0.0008	0.0021	0.1989	0.0194	0.0008
Fl$_{25}$−Ga$_{22}$	96	0.0135	0.0374	−0.0082	−0.0001	0.0082	4.9630	0.0605	0.0001

[a]All parameters: $\rho(r)$, $V^2\rho r$, $V(r)$, $K(r)$, $G(r)$, ε, ELF, and $H(r)$ are in au.

interactions. Notably, the electron density for the minimum, maximum, or saddle point is associated with atomic critical point (ACP), bond critical point (BCP), and ring critical point (RCP). The topological parameters like electron density ($\rho(r)$), energy density ($H(r)$), Laplacian of electron density ($\nabla^2\rho(r)$), kinetic electron density $G(r)$, potential electron density $V(r)$, bond ellipticity index (ε), and ELF used for the QTAIM analyses are obtained upon optimization of the system and listed in Table 5. The electron kinetic energy density $G(r)$, the electron potential energy density, and $\nabla^2\rho(r)$ are related by the virial theorem stated as shown in eq 2.[39−41]

$$\frac{1}{4}\nabla^2\rho(r) = 2G(r) + V(r) \tag{2}$$

QTAIM analysis is used in the study to better understand the nature and strength of interaction between the drug and the nanocluster surfaces. The visual representations of the interactions are displayed in Figure 6. According to QTAIM theory, a positive value for Laplacian $\nabla^2\rho(r)$ signifies noncovalent interaction while a negative value describes a covalent nature of interaction. As seen in Table 5, it is noteworthy that the positive $\nabla^2\rho(r)$ values reported for all observed interactions suggest a noncovalent nature of interaction. According to literature reports by Koch and Popelier,[42] when the square of the Laplacian of electron density is less than zero ($\nabla^2\rho(r)$ <0) and the energy density ($H(r)$) is less than zero ($H(r)$ < 0), such an interaction signifies a covalent (shared) interaction, while the noncovalent (closed shell) interaction emanating from the weak hydrogen bond, van der Waal's interaction, and electrostatic interaction is observed when $\nabla^2\rho(r)$ > 0 and $H(r)$ > 0. However, $\nabla^2\rho(r)$ > 0 and $H(r)$ <0 result in a partially covalent interaction. As shown in Table 5, a noncovalent interaction is clear in the Dic@F^{en}Ga$_{12}$As$_{12}$ interaction. Although other interactions were
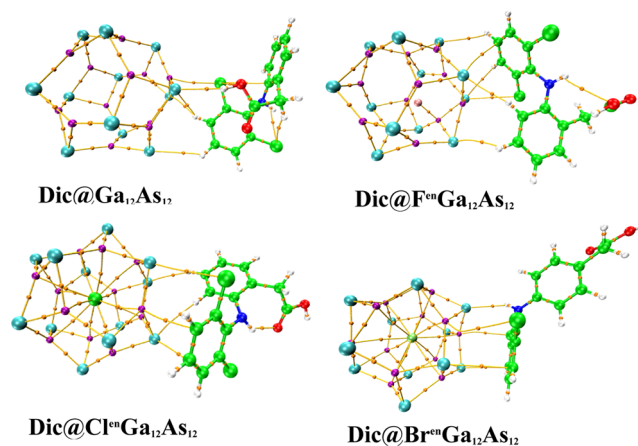
Figure 6. AIM plots showing bond critical points of the interaction between the adsorbate and adsorbent, respectively. The yellow dots designate different bond critical points, respectively.

dominantly noncovalent, partially covalent interactions were also observed for specific bond critical points: the BCP between Ga$_{21}$−Cl$_{54}$ and As$_8$−H$_{52}$ as observed for Dic@Ga$_{12}$As$_{12}$ and the BCP between the Br$_{25}$−Ga$_{15}$ and Ga$_{23}$−Cl$_{25}$ bonds in Dic@BenGa$_{12}$As$_{12}$ and Dic@Cl^{en}Ga$_{12}$As$_{12}$, respectively. The highest energy density value $H(r)$ of 0.0311 was observed for the As$_7$−Cl$_{54}$ bond in the F-encapsulated nanosurface (Dic@F^{en}Ga$_{12}$As$_{12}$), whereas the lowest energy density for the noncovalent interaction was observed in the same nanocluster at the bond critical point between the Fl$_{25}$−Ga$_{22}$ bond. These results are comparable with some other reported literature on B$_{12}$N$_{12}$ derivatives, in which a decrease in charge density was observed between the adsorbate and adsorbent fragments.[43] Also, the interaction between tabun and Al$_{12}$P$_{12}$, C$_{24}$, B$_{12}$N$_{12}$, and C$_{12}$Si$_{12}$, as revealed by QTAIM,
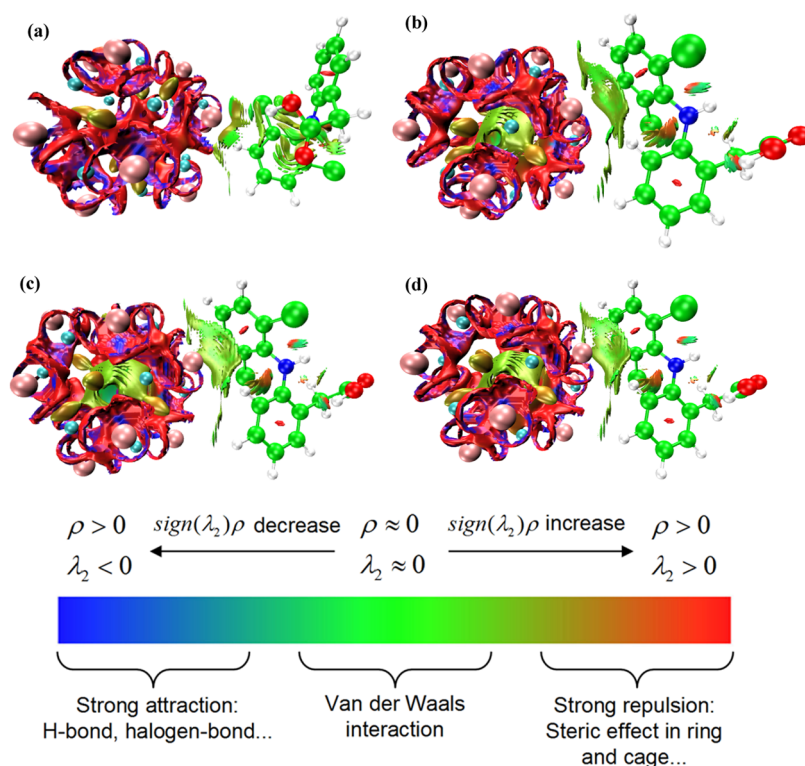
Figure 7. Visualized noncovalent interaction for the respective systems. (a–d) Dic@Ga$_{12}$As$_{12}$, Dic@F^{en}Ga$_{12}$As$_{12}$, Dic@Cl^{en}Ga$_{12}$As$_{12}$, and Dic@Br^{en}Ga$_{12}$As$_{12}$.

for similar tetragonal and hexagonal bonds disclosed that the nature of interaction for Al$_{12}$P$_{12}$ and C$_{24}$ bonds was van der Waals type while that for B$_{12}$N$_{12}$ and C$_{12}$Si$_{12}$ was observed to be van der Waals and weak covalent $(2 > V/G > 1)$.[44−46] The ELF value range is always between 0 and 1; however, when ELF has a value >0.5 and <1, it denotes the delocalization of electron density. ELF <0.5 deduces the presence of a noncovalent (closed shell) interaction, whereas ELF > 0.5 suggests a covalent (shared) interaction between the chemical bonds. Noticeably, the ELF values for the interactions listed in Table 5 show that the noncovalent interaction was dominant for the entire complexes under investigation. The Dic@Br^{en}Ga$_{12}$As$_{12}$ interaction recorded the highest ELF value at the BCP As$_4$−Cl$_{55}$ bond, with the lowest at BCP As$_9$−C$_{29}$ for the F-encapsulated nanocluster. The ELF data suggests that both the bare and encapsulated Ga$_{12}$As$_{12}$ strongly displayed noncovalent interaction and disclosed high affinity for the adsorbate molecule. Bond ellipticity is the topological parameter that provides information on the stability of a bond, and the Cl-encapsulated nanosurface (Dic@Cl^{en}Ga$_{12}$As$_{12}$) exhibited a more stable adsorption interaction than other surfaces, which is also disclosed by the ellipticity index. Although substantial stability of interaction was observed in other cases, the ellipticity index was quite lower, which conforms with previous assays.

3.7. Noncovalent Interaction. To gain further insight into the nature and type of intermolecular interactions between the adsorbate and adsorbent, the NCI is further invoked to this end. The NCI approach utilized is based on the reduced density gradient (RDG), which is a real space wave function analysis capable of quantifying both strength and type of noncovalent interaction exhibited during the adsorption process.[47] The NCI works based on the sign of the second

eigen function (λ_2) as well as the electron density gradient $\rho(r)$. The RDG isosurface maps are exhibited in Figure 7, and the plots are obtained at 0.5 au isosurface. Generally, the intuition from NCI analysis could be obtained based on the verdicts that the sign of the second eigen function of less than zero $(sign(\lambda_2)\rho(r) < 0)$ constitutes strong attraction and this is exhibited by blue color isosurface, whereas the van der Waal's interaction is visible when the sign of the second eigen function is approximately equal to zero $(sign(\lambda_2)\rho(r) \approx 0)$. Nonetheless, substantial repulsive interactions are prominent when the sign of the second eigen function is greater than zero $((\lambda_2)\rho(r) > 0)$; this is often exhibited by the red color isosurface. Based on this premise, it is ostensible that the prominent interaction exhibited by the adsorbent and adsorbate is the van der Waals interaction, which is visible by the green isosurface slab in Figure 7. However, the intensity of the green slab is more pronounced in the halogen-encapsulated nanoclusters as visible by the green isosurface than in the bare nanosurface. In all cases, weak intramolecular hydrogen bonds are visible by the blue spikes within the nanocages. The intuition from this analysis is that the complexes are stabilized by van der Waals and hydrogen bonding interactions, and hence, the proposed nanosensor surfaces are efficient in detecting the adsorbate molecule.

3.8. Electronic Sensor Properties. Two distinctive parameters, work function (Φ) and E_g, were employed to investigate the sensitivity of the proposed engineered Ga$_{12}$As$_{12}$ nanocluster toward diclofenac (Dic). The following relationship exists between the E_g and the population of conduction electrons[41]

$$N = AT^{3/2} \exp\left(-\frac{E_g}{2kT}\right)$$

(3)

Table 6. Calculated Fermi Level (E_f), Work Function (ϕ) Values in eV, and the Percentage Variation of Energy Gap (% ΔE_g) and Φ, with Respect to $Ga_{12}As_{12}$ and Encapsulated $Ga_{12}As_{12}$ Systems Studied[a]

modeled systems	%ΔE_g	E_f (eV)	Φ (eV)	%$\Delta\phi$	τ (s)
Dic@$Ga_{12}As_{12}$	0.256	−2.767	2.767	−10.256	2.872×10^{-13}
Dic@$F^{en}Ga_{12}As_{12}$	−20.835	−2.190	2.190	−20.835	2.120×10^{-11}
Dic@$Br^{en}Ga_{12}As_{12}$	−20.906	−2.188	2.188	−20.907	1.999×10^{-12}
Dic@$Cl^{en}Ga_{12}As_{12}$	−16.542	−2.244	2.244	−18.897	4.869×10^{-9}

[a]As tabulated, the energy of the Fermi level (E_F) and work function (Φ), all expressed in electron volts, (eV) are the requisite key parameters for analyzing a chemical sensor material. As such, the %ΔE_g and %$\Delta\Phi$ reflect the change in E_g and Φ after the adsorption process.

where k is the Boltzmann's constant (2.0×10^{-3} kcal/mol·K) and A (electron/m^3·$K^{3/2}$) is a constant. Numerous studies[48−52] revealed an agreement between this equation and the experimental findings. According to eq 2, the conduction electron population will change exponentially if the E_g of the adsorbent changes following the adsorption of a chemical agent. As such, this alters the adsorbent's electrical conductance, producing an electrical signal that may be useful in the detection of the chemical agent. Additionally, the influence of the adsorbate molecule was examined based on Φ and Fermi levels of the different investigated nanoclusters, as these are the key components of sensors that rely on Φ variations. The adsorbate might alter the examined systems' Φ and Fermi levels, which would alter the electron field emission current from the designed Dic@$Ga_{12}As_{12}$ surface and the encapsulated $Ga_{12}As_{12}$ nanosystems. In tandem, the gate voltage will vary if a chemical changes Φ of the sensors, which generates an electrical signal.[30]

The energy required to remove an electron from the Fermi level is referred to as Φ

$$\phi = V_{el(+\infty)} - E_F \equiv (-E_F) \qquad (4)$$

where $V_{el(+\infty)}$ is the electron electrostatic potential energy that is assumed to be zero, as its energy is far from the material's surface. Thus, as $V_{el(+\infty)} = 0$, Φ can be mathematically written as $-E_F$. Hence, the thermodynamic work necessary to add one electron to a solid-state entity is known as the Fermi level.[53] At $T = 0$ K, the usual assumption for the Fermi level is that it is localized in the middle of the energy gap (E_g) between the highest-occupied molecular orbital (HOMO) and the lowest-unoccupied molecular orbital (LUMO). It is crucial to note that the chemical potential, which corresponds to the Fermi level of the systems under consideration in this work, is what resides in the middle of the energy gap (E_g). This is because the chemical potential of a free gas of electrons is equal to its Fermi level according to the conventional definition. Thus, the Fermi level energy was calculated using the following equation

$$E_F = E_{HOMO} + \left(\frac{E_{LUMO} - E_{HOMO}}{2}\right) \equiv -\chi \qquad (5)$$

It is well known that altering the Fermi level and Φ will have the following effects on the electron emission from the surface of the systems (j) under study, as shown in the preceding equation

$$j = AT^2 e^{(-\Phi/kT)} \qquad (6)$$

where A is the Richardson constant (A/m^2) and T is the temperature (K). Correspondingly, after the adsorption of the adsorbate (Dic) molecule in the most stable complex, the HOMO of the studied $Ga_{12}As_{12}$ nanocluster is expressively affected, while the work function changed diminutively, as

depicted in Table 6. The LUMO somewhat destabilizes by shifting from −2.379 to −0.130 eV, and the HOMO also destabilizes by roughly 0.30 eV from −7.899 eV in the undecorated $Ga_{12}As_{12}$ nanocluster to −4.618 eV in the Dic@$F^{en}Ga_{12}As_{12}$ complex (Table 6). The partial DOS plot in Figure 5 also depicts the correlation that a new electronic state is generated (after adsorption) through the $Ga_{12}As_{12}$ nanocluster's E_g, which is primarily derived from the adsorbate molecule (Dic).

Additionally, the molecular shape of the HOMO level of the $Cl^{en}Ga_{12}As_{12}$ complex shows vividly that the HOMO orbital is localized on the nanosurface, as illustrated in Figure 4. While the LUMO is still located specifically on the $Cl^{en}Ga_{12}As_{12}$ surface, as is the case with the other engineered encapsulated $Ga_{12}As_{12}$ nanoclusters under study. Hence, the slight shift of the HOMO level from the surface of $Ga_{12}As_{12}$ to the surface of the drug is in good agreement with the large HOMO energy change (Figure 4). The new state in the complexes E_g, however, shows that diclofenac's adsorption on the surface of the $Ga_{12}As_{12}$ nanocluster causes the E_g to decrease from 5.520 eV in the $Ga_{12}As_{12}$ nanocluster to 4.618 eV in the complex (Dic@$Ga_{12}As_{12}$). According to eq 5, the change in E_g considerably increases the electrical conductance of the $Ga_{12}As_{12}$ nanocluster. As such, certain electronic sensors rely on the variations in electrical conductivity brought on by the adsorption process because they provide an electrical signal. As such, a pivotal conclusion can be drawn that the $Ga_{12}As_{12}$ nanocluster might be an interesting option for an electronic sensor for diclofenac detection. As the work function of the $Ga_{12}As_{12}$ nanocluster is not changed noticeably during the adsorption process, we do not suggest this nanocluster as a Φ-type sensor.

3.9. Recovery Time. The recovery time (τ), the time necessary for the desorption of adsorbate from an adsorbent, is another pivotal fundamental parameter in the field of nanosensing. As Dic-adsorbed structures have attained considerably more energetic and substantial stability, it is indispensable to calculate the desorption time of the adsorbate from the adsorbent to effectively project the most efficient nanosensor material toward the studied molecule. More so, strong interactions make the desorption process challenging, and interaction strength is a crucial factor in the development of sensors. However, if the adsorption energy shifts more negatively, as evident in Dic@$Cl^{en}Ga_{12}As_{12}$, a longer recovery period would be anticipated. The recovery time is computed based on eq 7[44−48]

$$\tau = \nu^{-1} e\left(\frac{-E_{ads}}{k_B T}\right) \qquad (7)$$

where ν, T, and k stand for the attempted frequency, the temperature in kelvin, and the Boltzmann constant (2.0×10^{-3}

kcal/mol·K), respectively. The various computed recovery times for the chemical systems studied are tabulated in Table 6. At normal temperature, the calculated τ for the Dic@$Cl^{en}Ga_{12}As_{12}$ surface is observed to be 4.869 ms, with vacuum ultraviolet light ($v_b \sim 10^{16}$ s^{-1}), which has been reported in various studies; thus, this nanosurface has the greatest interaction. With respect to Table 6, it can be deduced that the computed recovery times for the adsorbed systems (Dic@$Ga_{12}As_{12}$, Dic@$F^{en}Ga_{12}As_{12}$, Dic@$Br^{en}Ga_{12}As_{12}$, Dic@$Cl^{en}Ga_{12}As_{12}$) are perceived to be 2.872, 2.120, 1.999, and 4.869 ms, respectively. Thus, expressly divulging that Dic@$Cl^{en}Ga_{12}As_{12}$ possesses the highest desorption time and therefore more suitable for detection purposes since its affinity for the adsorbed molecule is high. This result is in tandem with previous findings, which disclosed the unfavorable nature of the interaction in Dic@$Br^{en}Ga_{12}As_{12}$ due to substantial deformation of the adsorbent surface. This nanosurface also has the least desorption time and thus not suitable for sensing purposes. The suitability of a chemical sensor must be such that the affinity of the surface toward the adsorbate is high enough to be detected even at minute concentrations; hence, a longer recovery time shows that the nanosensor strongly interacted with the surface and its presence can be detected regardless of temperature or environmental factors. To clarify any issues concerning the removal of the studied material from the environment after use, it is worth mentioning that the studied nanomaterials are more appropriate for the fabrication of electronic sensor devices based on the results of the sensor mechanism and conductivity. Thus, the need for dissolution of the clusters in solution is limited and hence, limiting also, the extent of environmental contamination after use.[54] Nevertheless, several methods have been proposed and utilized to effectively eradicate and recycle GaAs particles from scrapped GaAs-based circuits. Recently, a hydrothermal-buffering method HBM was developed by Zhan and co-workers,[55,56] about 99.9 and 96.5% recovery rates of GaAs were recovered, and the method was proven to be environmentally friendly.

4. CONCLUSIONS

With the aim of assessing the efficacy of GaAs and its encapsulated derivatives to sense and adsorb diclofenac, the structural and electronic sensitivity of engineered nanoclusters toward diclofenac has been successfully investigated and reported in this work by employing the meta-generalized gradient method based on density functional theory (ωB97XD/def2-SVP). Electronic properties such as conductivity, adsorption energy, natural bond orbital, work function, deformation energy, thermodynamics of adsorption, recovery time as well as topological analysis based on QTAIM, and NCI have been utilized to give the verdicts of the efficacy of the engineered nanoclusters as nanosensors for diclofenac. We found that the adsorbate molecule preferred to be adsorbed via the electropositive hydrogen atoms of the aromatic ring by assuming a flat orientation on top of the As sites of the nanocluster. Substantial stability was also predicted by electronic descriptors, and no dramatic deformation by breakage or geometry was observed during the adsorption process. The energy gap of the nanoclusters was observed to be influenced by engineering with halogens via encapsulation as well as during the adsorption process. Specifically, the energy gap increased slightly because of encapsulation with the halogens, whereas the energy gap decreased considerably during adsorption from 5.858 to 4.488 eV in Dic@

$Cl^{en}Ga_{12}As_{12}$ and 5.836 to 4.376 eV in the case of Dic@$Br^{en}Ga_{12}As_{12}$. This variation in energy gap disclosed that the electrical conductivity of the nanoclusters is enhanced and will be readily converted to an electrical signal. Therefore, Dic@$Cl^{en}Ga_{12}As_{12}$ is proposed as the most suitable engineered nanocluster for detecting the adsorbate molecule. This nanocluster was also predicted to have a short recovery time of about 4.869 ms to desorb the adsorbate molecule (Dic) from the surface. Also, encapsulation with halogens was observed to be a successful approach to improve the sensing attributes of the $Ga_{12}As_{12}$ nanocluster under consideration as substantial enhancement in electrical properties, stability, as well as adsorption feasibility, was ensured by virtue of encapsulation. To appraise the nature of interaction between the adsorbate and adsorbent, topological analysis was conducted to this end; hence, the findings show that the dominant stabilization interaction between the adsorbate and adsorbent is the van der Waals interaction while the nature of interaction was demonstrated to be strongly noncovalent. Therefore, the affinity of the nanoclusters toward the adsorbed molecule is high and thus advantageous for the construction of sensor devices. Also, the economical consideration of using GaAs nanoclusters is sustainable; reports show that Ga-based semiconducting materials are relatively cheaper and sustainable when compared to other transition metal-based counterparts.

■ ASSOCIATED CONTENT

Ⓢ Supporting Information

The Supporting Information is available free of charge at https://pubs.acs.org/doi/10.1021/acsomega.2c06097.

> Figures S1−S4 contain the coordinates for quantum mechanical calculations. The other adsorption configurations of the prerelaxed geometry are depicted in Figure S6. Figure S7 depicts the projected density of states for the adsorbed systems. Table S1 depicts the BSSE and complexation energies of the studied complexes (PDF)

■ AUTHOR INFORMATION

Corresponding Authors

Hitler Louis − *Computational and Bio-Simulation Research Group, University of Calabar, Calabar 540221, Nigeria; Department of Pure and Applied Chemistry, University of Calabar, Calabar 540221, Nigeria;* ⓘ orcid.org/0000-0002-0286-2865; Email: louismuzong@gmail.com

Tomsmith O. Unimuke − *Computational and Bio-Simulation Research Group, University of Calabar, Calabar 540221, Nigeria; Department of Pure and Applied Chemistry, University of Calabar, Calabar 540221, Nigeria;* ⓘ orcid.org/0000-0001-8721-2345; Email: ojtomtsm@gmail.com

Authors

Ikechukwu C. Nwobodo − *Computational and Bio-Simulation Research Group, University of Calabar, Calabar 540221, Nigeria; Department of Pure and Applied Chemistry, University of Calabar, Calabar 540221, Nigeria*

Onyinye J. Ikenyirimba − *Department of Chemistry Education, Alex Ekwueme Federal University, Abakaliki, Ebonyi State 010, Nigeria;* ⓘ orcid.org/0000-0002-1038-1076

Anthony C. Iloanya − *Department of Physics, Lehigh University, Bethlehem, Pennsylvania 18015, United States*

Gideon E. Mathias − *Computational and Bio-Simulation Research Group, University of Calabar, Calabar 540221, Nigeria; Department of Pure and Applied Chemistry, University of Calabar, Calabar 540221, Nigeria*

Vincent N. Osabor − *Department of Pure and Applied Chemistry, University of Calabar, Calabar 540221, Nigeria*

Eze F. Ahuekwe − *Computational and Bio-Simulation Research Group, University of Calabar, Calabar 540221, Nigeria; Department of Biological Sciences, Covenant University, Ota 112104 Ogun State, Nigeria*

Adedapo S. Adeyinka − *Research Centre for Synthesis and Catalysis, Department of Chemical Sciences, University of Johannesburg, Johannesburg 2006, South Africa*

Complete contact information is available at:
https://pubs.acs.org/10.1021/acsomega.2c06097

Author Contributions

I.C.N.: Analysis, investigation, and manuscript first draft., H.L.: conceptualization, design, supervision, and editing. T.O.U.: validation, investigation, analysis, writing, review, editing, and manuscript final draft; O.J.I.: analysis and writing; A.C.I.: data curation, analysis, and writing; G.E.M.: analysis and writing; V.N.O.: supervision, review, and editing; E.F.A.: analysis, writing, and editing; A.S.A.: methodology, editing, and resources.

Notes

The authors declare no competing financial interest.
All data generated or analyzed during this study are included within this article and its Supporting Information.

■ ACKNOWLEDGMENTS

■ REFERENCES

(1) Galisteo, A.; Jannus, F.; Garcia-Garcia, A.; Aheget, H.; Rojas, S.; Lupianez, J. A.; Rodriguez-Dieguez, A.; Reyes-Zurita, F. J.; Quilez del Moral, F. J. Diclofenac N-Derivatives as therapeutic agents with anti-inflammatory and anti-cancer effect. *Int. J. Mol. Sci.* **2021**, *22*, 5067.

(2) Kaczmarek-Kędziera, A. Gas Phase Computational Study of Diclofenac Adsorption on Chitosan Materials. *Molecules* **2020**, *25*, 2549.

(3) Moser, P.; Sallmann, A.; Wiensenberg, I. Synthesis and quantitative structure-activity relationships of diclofenac analogs. *J. Med. Chem.* **1990**, *33*, 2358−2368.

(4) Altman, R.; Bosch, B.; Brune, K.; Patrignani, P.; Young, C. Advances in NSAID development: evolution of diclofenac products using pharmaceutical technology. *Drugs* **2015**, *75*, 859−877.

(5) McGettigan, P.; Henry, D. Use of non-steroidal anti-inflammatory drugs that elevate cardiovascular risk: an examination of sales and essential medicines lists in low-, middle-, and high-income countries. *PLoS Med.* **2013**, *10*, No. e1001388.

(6) Arga, Z.; Sabzwari, S. R. A.; Vargova, V. Cardiovascular Risk of Nonsteroidal Anti-Inflammatory Drugs: An Under-Recognized Public Health Issue. *Cureus* **2017**, *9*, No. e1144.

(7) Brodin, T.; Piovano, S.; Fick, J.; Klaminder, J.; Heynen, M.; Jonsson, M. Ecological effects of pharmaceuticals in aquatic systems– impacts through behavioural alterations. *Philos. Trans. R. Soc. Lond., B: Biol. Sci.* **2014**, *369*, No. 20130580.

(8) Kaczala, F.; Blum, S. E. The Occurrence of Veterinary Pharmaceuticals in the Environment: A Review. *Curr. Anal. Chem.* **2016**, *12*, 169−182.

(9) Marjoribanks, J.; Ayeleke, R. O.; Farquhar, C.; Proctor, M. Nonsteroidal anti-inflammatory drugs for dysmenorrhoea. *Cochrane Database Syst. Rev.* **2015**, *7*, No. CD001751.

(10) Tiwari, S. K.; Sahoo, S.; Wang, N.; Huczko, A. Graphene research and their outputs: Status and prospect. *J. Sci. Adv. Mater. Dev.* **2020**, *5*, 10−29.

(11) Novoselov, K. S.; Fal'ko, V. I.; Colombo, L.; Gellert, P. R.; Schwab, M. G.; Kim, K. A roadmap for graphene. *Nature* **2012**, *490*, 192−200.

(12) Harish, V.; Tewari, D.; Gaur, M.; Yadav, A. B.; Swaroop, S.; Bechelany, M.; Barhoum, A. Review on Nanoparticles and Nano-structured Materials: Bioimaging, Biosensing, Drug Delivery, Tissue Engineering, Antimicrobial, and Agro-Food Applications. *Nanomaterials* **2022**, *12*, 457.

(13) Akinsiku, A. A.; Ajani, O. O.; Adekoya, J. A.; Emetere, M. E.; Dare, E. O. Green synthesis of triclinic (anorthic) phase AgCoPO4 nanoparticles: optical studies and theoretical modelling. *Heliyon* **2020**, *6*, No. e05029.

(14) Sun, Y. F.; Liu, S. B.; Meng, F. L.; Liu, J. Y.; Jin, Z.; Kong, L. T.; Liu, J. H. Metal oxide nanostructures and their gas sensing properties: a review. *Sensors* **2012**, *12*, 2610−2631.

(15) Lim, T.; Ring, T. A.; Zhang, H. Chemical analysis of the Gallium surface in a physiologic buffer. *Langmuir* **2022**, *38*, 6817−6825.

(16) Li, Z.; Sun, J.; Huang, Y.; Liu, Y.; Xu, J.; Chen, Y.; Liang, L.; Li, J.; Liao, Q.; Li, S.; Zhou, K. A Nanomicellar Prodrug Carrier Based on Ibuprofen-Conjugated Polymer for Co-delivery of Doxorubicin. *Front. Pharmacol.* **2018**, *9*, 781.

(17) Tonel, M. Z.; Martins, O. M.; Zanella, I.; Pontes, B. R.; Fagan, S. B. A first principles study of the interaction of doxorubicin with graphene. *Comput. Theor. Chem.* **2017**, *1115*, 270−275.

(18) Mirkamali, E. S.; Ahmadi, R. Adsorption of melphalan anticancer drug on the surface of boron nitride cage (B12N12): A comprehensive DFT study. *J. Med. Chem. Sci.* **2020**, *3*, 199−207.

(19) Veeralingam, S.; Badhulika, S. Two-dimensional metallic NiSe2 nanoclusters−based low-cost, flexible, amperometric sensor for detection of neurological drug carbamazepine in human sweat samples. *Front. Chem.* **2020**, *8*, 337.

(20) Yen, Y. K.; Capua, E.; Naaman, R. Application of a GaAs-based sensor for detecting hemoglobin in gastrointestinal environments. *IEEE Sens. J.* **2017**, *17*, 660−666.

(21) Mohammadi, M. D.; Abdullah, H. Y.; Louis, H.; Mathias, G. E. 2D boron nitride material as a sensor for H2SiCl2. *Comput. Theor. Chem.* **2022**, *1213*, No. 113742.

(22) Tsuzuki, S.; Uchimaru, T. Accuracy of intermolecular interaction energies, particularly those of hetero-atom containing molecules obtained by DFT calculations with Grimme's D2, D3 and D3BJ dispersion corrections. *Phys. Chem. Chem. Phys.* **2020**, *22*, 22508−22519.

(23) Chai, J.-D.; Martin, H.-G. "Long-range corrected hybrid density functionals with damped atom-atom dispersion corrections.". *Phys. Chem. Chem. Phys.* **2008**, *10*, 6615−6620.

(24) Frisch, M. J.; Trucks, G. W.; Schlegel, H. B.; Scuseria, G. E.; Robb, M. A.; Cheeseman, J. R.; Scalmani, G.; Barone, V.; Petersson, G. A.; Nakatsuji, H.; Li, X.; Caricato, M.; Marenich, A. V.; Bloino, J.; Janesko, B. G.; Gomperts, R.; Mennucci, B.; Hratchian, H. P.; Ortiz, J. V.; Izmaylov, A. F.; Sonnenberg, J. L.; Williams, E.; Ding, F.; Lipparini, F.; Egidi, F.; Goings, J.; Peng, B.; Petrone, A.; Henderson, T.; Ranasinghe, D.; Zakrzewski, V. G.; Gao, J.; Rega, N.; Zheng, G.; Liang, W.; Hada, M.; Ehara, M.; Toyota, K.; Fukuda, R.; Hasegawa, J.; Ishida, M.; Nakajima, T.; Honda, Y.; Kitao, O.; Nakai, H.; Vreven, T.; Throssell, K.; Montgomery, J. A., Jr.; Peralta, J. E.; Ogliaro, F.; Bearpark, M. J.; Heyd, J. J.; Brothers, E. N.; Kudin, K. N.; Staroverov, V. N.; Keith, T. A.; Kobayashi, R.; Normand, J.; Raghavachari, K.; Rendell, A. P.; Burant, J. C.; Iyengar, S. S.; Tomasi, J.; Cossi, M.; Millam, J. M.; Klene, M.; Adamo, C.; Cammi, R.; Ochterski, J. W.;

Martin, R. L.; Morokuma, K.; Farkas, O.; Foresman, J. B.; Fox, D. J.*Gaussian 16*, revision C.01; Gaussian Inc.: Wallingford, CT, 2016.

(25) Glendening, E. D.; Reed, A. E.; Carpenter, J. E.; Weinhold, F.*NBO*, version 3.1; Gaussian Inc.: Pittsburgh, PA, 2003.

(26) Lu, T.; Chen, F. Multiwfn: a multifunctional wavefunction analyzer. *J. Comput. Chem.* **2012**, *33*, 580−592.

(27) O'boyle, N. M.; Tenderholt, A. L.; Langner, K. M. Cclib: A Library for Package-Independent Computational Chemistry Algorithms. *J. Comput. Chem.* **2008**, *29*, 839−845.

(28) Humphrey, W.; Dalke, A.; Schulten, K. VMD: Visual Molecular Dynamics. *J. Mol. Graphics* **1996**, *14*, 33−38.

(29) Louis, H.; Mathias, G. E.; Ikenyirimba, O. J.; Unimuke, T. O.; Etiese, D.; Adeyinke, A. S. Metal-doped Al12N12X (X= Na, Mg, K) Nanoclusters as Nanosensors for Corboplatin: Insight from first-principles computation. *J. Phys. Chem. B* **2022**, *126*, 5066−5080.

(30) van Duijneveldt, F. B.; Jeanne, G. C. M.; Van Lenthe, J. H. State of the art in counterpoise theory. *Chem. Rev.* **1994**, *94*, 1873−1885.

(31) Boys, S. F.; Bernardi, F. Calculation of Small Molecular Interactions by Differnces of Separate Total Energies-Some Procedures with Reduced Errors. *Mol. Phys.* **1970**, *19*, 553.

(32) Simon, S.; Duran, M.; Dannenberg, J. J. "How does basis set superposition error change the potential surfaces for hydrogen bonded dimers?,". *J. Chem. Phys.* **1996**, *105*, 11024−11031.

(33) Rosch, N.*Counterpoise Correction*; Quantum Chemistry Laboratory, Technical University of Munich, 2022.

(34) Unimuke, T. O.; Louis, H.; Eno, E. A.; Agwamba, E. C.; Adeyinka, A. S. Meta-Hybrid Density Functional Theory Prediction of the Reactivity, Stability, and IGM of Azepane, Oxepane, Thiepane, and Halogenated Cycloheptane. *ACS Omega* **2022**, *7*, 13704−13720.

(35) Toriyama, M. Y.; Ganose, A. M.; Dylla, M.; Anand, S.; Park, J.; Brod, K. M.; Munro, J. M.; Persson, K. A.; Jain, A.; Snyder, J. How to analyse a density of states. *Mater. Today Electron.* **2022**, *1*, No. 100002.

(36) Nguyen, C. H.; Field, J. A.; Sierra-Alvarez, R. Microbial toxicity of gallium- and indium-based oxide and arsenide nanoparticles. *J. Environ. Sci. Health, Part A* **2020**, *55*, 168−178.

(37) Zeng, C.; Gonzalez-Alvarez, A.; Orenstein, E.; Field, J. A.; Shadman, F.; Sierra-Alvarez, R. Ecotoxicity assessment of ionic As(III), As(V), In(III) and Ga(III) species potentially released from novel III-V semiconductor materials. *Ecotoxicol. Environ. Saf.* **2017**, *140*, 30−36.

(38) Bader, R. F. W. Atoms in molecules. *Acc. Chem. Res.* **1985**, *18*, 9−15.

(39) Arnold, W. D.; Oldfield, E. The chemical nature of hydrogen bonding in proteins via NMR: J-Couplings, chemical shifts, and AIM theory. *J. Am. Chem. Soc.* **2000**, *122*, 12835−12841.

(40) Mohammadi, M. D.; Abbas, F.; Louis, H.; Mathias, G. E.; Unimuke, T. O. Trapping of CO, CO2, H2S, NH3, NO, NO2, and SO2 by polyoxometalate compound. *Comput. Theor. Chem.* **2022**, *1215*, No. 113826.

(41) Jaziri, E.; Louis, H.; Gharbi, C.; Unimuke, T. O.; Agwamba, E. C.; Mathias, G. E.; Fugita, W.; Nasr, C. B.; Khedhiri, L. Synthesis, X-ray crystallography, molecular electronic property investigation, and leukopoiesis activity of novel 4,6-dimethyl-1,6-dihydropyridin-2-amino nitrate hybrid material. *J. Mol. Struct.* **2022**, *1268*, No. 133733.

(42) Koch, U.; Popelier, P. L. Characterization of CHO hydrogen bonds on the basis of the charge density. *J. Phys. Chem. A* **1995**, *99*, 9747−9754.

(43) Mohammadi, M. D.; Salih, I. H.; Abdullah, H. Y. The Adsorption of Chlorofluoromethane on Pristine and Ge-doped silicon carbide Nanotube: a PBC-DFT, NBO, and QTAIM study. *Mol. Simul.* **2020**, *46*, 1405−1416.

(44) Padash, R.; Esfahani, M. R.; Rad, A. S. The computational quantum mechanical study of sulfamide drug adsorption onto X12Y12 Fullerene-like nanocages: detailed DFT and QTAIM investigations. *J. Biomol. Struct. Dyn.* **2021**, *39*, 5427−5437.

(45) Fallahi, P.; Jouypazadeh, H.; Farrokhpour, H. Theoretical studies on the potentials of some nanocages (Al12N12, Al12P12, B12N12, Be12O12, C12Si12, Mg12O12 and C24) on the detection and adsorption of Tabun molecule: DFT and TD-DFT study. *Mol. Liq.* **2017**, *240*, 138−148.

(46) Louis, H.; Ikenyirimba, O. J.; Unimuke, T. O.; Mathias, G. E.; Gber, T. E.; Adeyinka, A. S. Electrocatalytic activity of metal encapsulated, doped, and engineered fullerene-based nanostructured materials towards hydrogen evolution reaction. *Sci. Rep.* **2022**, *12*, No. 15608.

(47) Soltani, A.; Raz, S. G.; Taghartapeh, M. R.; Moradi, A. V.; Mehrabian, R. Z. Ab Initio Study of the NO2 and SO2 Adsorption on Al12N12 Nano-cage Sensitized with Gallium and Magnesium. *Comput. Mater. Sci.* **2013**, *79*, 795−803.

(48) Sajid, H.; Siddique, S. A.; Ahmed, E.; Arshad, M.; Gilani, M. A.; Rauf, A.; Imran, M.; Mahmood, T. DFT outcome for Comparative Analysis of Be12O12, Mg12O12 and Ca12O12 Nanocages toward Sensing of N2O, NO2, NO, H2S, SO2 and SO3 gases. *Comput. Theor. Chem.* **2022**, *1211*, No. 113694.

(49) Nemati-Kande, E.; Karimian, R.; Goodarzi, V.; Ghazizadeh, E. Feasibility of Pristine, Al-doped and Ga-doped Boron Nitride nanotubes for Detecting SF4 gas: A DFT, NBO and QTAIM Investigation. *Appl. Surf. Sci.* **2020**, *510*, No. 145490.

(50) Louis, H.; Amodu, I. O.; Unimuke, T. O.; Gber, T. E.; Isang, B. B.; Adeyinka, A. S. Modeling of Ca12O12, Mg12O12 and Al12N12 nanostructured materials as sensors for phosgene (Cl2CO). *Mater. Today Commun.* **2022**, *32*, No. 103946.

(51) Egemonye, T. C.; Louis, H.; Unimuke, T. O.; Gber, T. E.; Edet, H. O.; Bassey, V. M.; Adeyinka, A. S. First principles density functional theory study on the electrochemical properties of cyclohexanone derivatives as organic carbonyl-based cathode material for lithium-ion batteries. *Arab. J. Chem.* **2022**, *15*, No. 104026.

(52) Hossain, M. R.; Hasan, M. M.; Shamim, S. U. D.; Ferdous, T.; Hossain, M. A.; Ahmed, F. First-Principles Study of the Adsorption of Chlormethine Anticancer Drug on C24, B12N12 and B12C6N6 Nanocages. *Comput. Theor. Chem.* **2021**, *1197*, No. 113156.

(53) Ganji, M. D.; Kiyani, H. Molecular simulation of efficient removal of H2S pollutant by cyclodextrine functionalized CNTs. *Sci. Rep.* **2019**, *9*, No. 10605.

(54) Hussain, S.; Chatha, S. A. S.; Hussain, A. I.; Hussain, R.; Yasir Mehboob, M.; Mansha, A.; Nabel, S.; Ayub, K. In Silico Designing of Mg12O12 Nanoclusters with a Late Transition Metal for NO2 Adsorption: An Efficient Approach toward the Development of NO2 Sensing Materials. *ACS Omega* **2021**, *6*, 14191−14199.

(55) Zhan, L.; Zhang, Y.; Ahmad, Z.; Xu, Z. Novel recycle technology for recovering Gallium Arsenide from scraped integrated circuits. *ACS Sustainable Chem. Eng.* **2020**, *8*, 2874−2882.

(56) Uryu, T.; Yoshinaga, J.; Yanagisawa, Y. Environmental fate of Gallium Arsenide semiconductor disposal: a case study of mobile phones. *J. Ind. Ecol.* **2003**, *7*, 103−112.